ARTICLE

Solar-driven tandem photoredox nickel-catalysed cross-coupling using modified carbon nitride

Received 00th January 20xx,
Accepted 00th January 20xx

DOI: 10.1039/x0xx00000x

Yangzhong Qin,[a]† Benjamin C. M. Martindale,[a]† Rui Sun,[a] Adam J. Rieth[a] and Daniel G. Nocera*[a]

Nickel-catalysed aryl amination and etherification are driven with sunlight using a surface-modified carbon nitride to extend the absorption of the photocatalyst into a wide range of the visible region. In contrast to traditional homogeneous photochemical methodologies, the lower cost and higher recyclability of the metal-free photocatalyst, along with the use of readily available sunlight, provides an efficient and sustainable approach to promote nickel-catalysed cross-couplings.

Introduction

Photoredox chemistry has expanded the toolbox of chemical transformations owing to the ability to generate high energy and reactive radical intermediates with facility under mild conditions.[1-6] Despite significant progress in the development of selective bond-breaking and -forming reactions resulting from photoredox-driven transformations using nickel, iron and copper complexes,[7-12] many of these contemporary methods rely on homogeneous photocatalysts based on iridium or ruthenium, which are expensive and potential sources of toxic contaminants.[13-16] Moreover, blue or UV light is often required to drive many photocatalytic reactions due to the limited absorption range of the common photocatalysts,[17-21] which can result in off-pathway side reactions due to the competing excitation of other photoactive species present in solution. For instance, bipyridine-ligated nickel aryl halide complexes, often formed in nickel-catalysed cross-couplings, can absorb UV and blue light and result in unproductive homocoupling and dehalogenation.[22,23]

Although photoredox catalysis provides powerful strategies and new capabilities for synthesis, the cost of the photocatalyst and light source, as well as the environmental footprint of the synthetic method and catalyst recovery have been infrequently considered. To address this shortcoming, Energy Intensity (EI = total process energy/mass of final product) is an essential metric for quantifying the sustainability of chemical processes in addition to the more commonly used Process Mass Intensity (PMI = mass of input material/mass of product),[24-26] which only considers the material input. For photocatalytic processes, energy and materials costs for generating photons, photocatalysts and products accounted for by including EI with PMI. Additionally, costs are accounted for associated with removing toxic residues of the photocatalysts and their subsequent processing as chemical waste, the failure of which may result in detrimental consequences for the environment and public health.[27-29] For example, the tolerable amount of metallic residues (e.g. platinum, iridium and ruthenium) in pharmaceuticals is strictly regulated. Therefore, strategies to drive chemical reactions with sustainable, recyclable and non-toxic materials are in high demand for improved energy efficiency, cost-effectiveness and minimal environmental impact.

Solar-driven chemical reactions are inherently sustainable and conducive towards a high EI.[3,30-32] Although the power of sunlight at sea level is relatively high, on the order of 1000 W/m^2 (based on ASTM G-173-03 standard), the energy is spectroscopically spread over a wide range from the UV region to the IR. Hence, an efficient photocatalyst that can maximally absorb broadband sunlight remains an unmet goal in

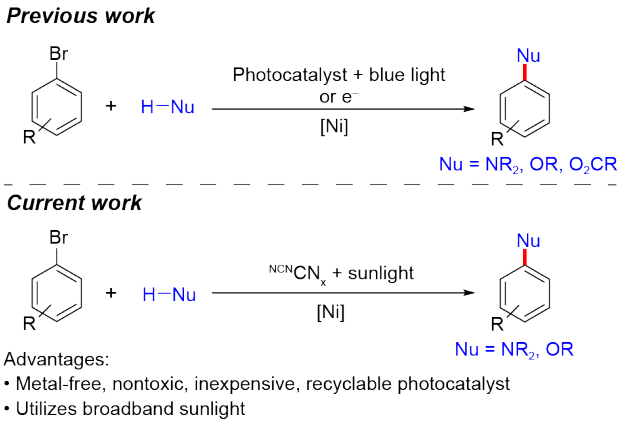

Scheme 1. Summary of previous and current work on nickel-catalysed cross-coupling.

[a] *Department of Chemistry and Chemical Biology, Harvard University, 12 Oxford Street, Cambridge, Massachusetts 02138, United States of America. Email: dnocera@fas.harvard.edu*

†These authors contribute equally.

Electronic Supplementary Information (ESI) available: [Details about methodologies and Measurements]. See DOI: 10.1039/x0xx00000x

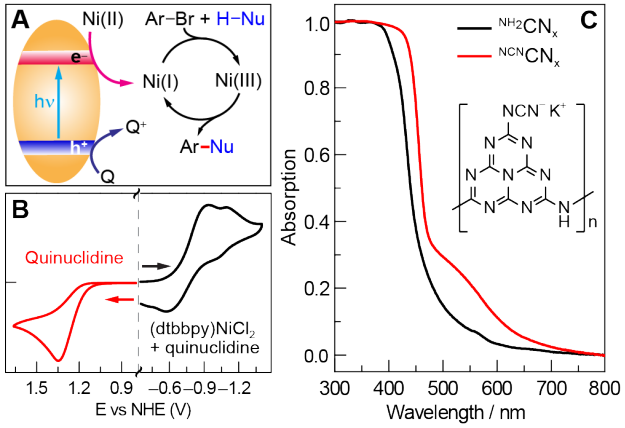

Figure 1. (**A**) A mechanistic scheme of the photoredox nickel-catalysed cross-coupling reaction. Q stands for quencher. (**B**) Cyclic voltammetry measurements of 2.5 mM (dtbbpy)$NiCl_2$ in the presence of 5 mM quinuclidine, and 12 mM quinuclidine in acetonitrile. (**C**) Absorption spectra of unmodified carbon nitride ($^{NH_2}CN_x$) and modified carbon nitride ($^{NCN}CN_x$). The inset shows a posited unit structure of $^{NCN}CN_x$.

photoredox catalysis. In contrast to homogeneous photocatalysts, semiconductors, such as GaAs and CdTe, can harness a broader wavelength of incident light; such materials appear to be promising photocatalysts for sustainable photocatalytic reactions.[33-36] Nonetheless, the use of inorganic semiconductor colloids to harness sunlight and directly drive chemical reactions has remained challenging due to a variety of factors, including, but not limited to, surface passivation, charge recombination, materials instability and the balance between electron-transfer kinetics from the conduction and valence bands.[36,37]

Cross-coupling between nucleophiles and aryl halides is a reaction that has employed both homogeneous and heterogeneous photocatalysts.[38-46] To date, these reactions have required intense light sources and/or prolonged illumination.[1-6,17-21] We now demonstrate that nickel-catalysed aryl amination (C–N) and etherification (C–O) may be directly driven by solar light using a surface-modified carbon nitride (Scheme 1), which extends absorption into a wide range of the visible region thus making it amenable for solar photoredox catalysis. Additionally, besides being metal-free, the modified carbon nitride is nontoxic, inexpensive, easily synthesized and easily separated from product mixtures.

Results and discussion

Photoredox nickel-catalysed aryl etherification was first reported with a polypyridyl iridium photocatalyst that is excited by blue LED light.[38] The mechanism was further studied by our group and revealed to involve a sustained productive Ni(I/III) dark cycle initiated by a one electron reduction of the Ni(II) precatalyst (Figure 1A).[47,48] Significantly, our recent study shows that the photoredox reaction can also be realized by replacing the photocatalyst and photon source with a sub-stoichiometric amount of Zn metal,[48] suggesting that the photocatalytic cycle serves as an electron source to return an off-cycle Ni(II) complex to the active Ni(I) catalyst. This observation is consonant with the recent observation that Ni(II) resides off-cycle in a resting state rather than an on-cycle catalyst.[49] These studies thoroughly explored the reaction conditions as well as the mechanism, which allowed us to employ optimized reaction conditions (see Table 1), and provide an underpinning for developing heterogeneous photocatalysts with attractive energy intensity.

Table 1. Testing C–O cross-coupling reactions with various heterogeneous photocatalysts.[a]

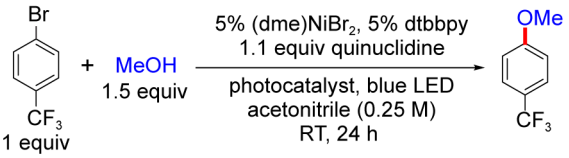

Photocatalyst	Band Gap (eV)	VB Potential (V)	CB Potential (V)	Yield (%)
SiC	3.0	1.5	–1.5	14
$^{NH_2}CN_x$	2.7	1.8	–0.9	92
ZnSe	2.7	0.8	–1.9	0
GaP	2.3	1.2	–1.1	24
CdTe	1.4	0.7	–0.7	3

[a] Reactions were run on a 2-mL scale with 8 mg of photocatalyst. The bandgap, valence band (VB) and conduction band (CB) potentials were taken from ref. 14, and all referenced to NHE at pH = 0.

A suite of heterogeneous catalysts comprising SiC, carbon nitride ($^{NH_2}CN_x$), ZnSe, GaP and CdTe was surveyed with band gaps ranging from 3.0 eV to 1.4 eV.[50-53] Table 1 illustrates the efficacy of the photocatalysts for C–O coupling under 40 W blue LED light (Figure S1) illumination. The product yield was determined by ^{1}H NMR spectroscopy using 1,3-benzodioxole as an internal standard. We found that $^{NH_2}CN_x$ gave the highest yield of product (92%) after 24 hours of illumination. ZnSe, possessing nearly the same band gap (2.7 eV) as $^{NH_2}CN_x$, yielded no product even though the conduction band is more reducing than that of $^{NH_2}CN_x$ (–1.9 V vs. –0.9 V as referenced to NHE at pH = 0, Table 1).[51,52] Although they possess similar band gaps, the valence band potential of ZnSe is 0.9 V as compared to 1.8 V for $^{NH_2}CN_x$, suggesting that the less oxidizing valence band of ZnSe may prevent it from driving photocatalysis. Consistent with this contention, GaP and SiC, which have higher oxidation potentials for their valence bands (1.2 V and 1.5 V, respectively) than that of ZnSe, showed modest conversion yields of 24% and 14%, respectively, after 24 hours of illumination under blue light. To provide further insight as to the reaction disparity among heterogeneous photocatalysts, we examined, by cyclic voltammetry (CV), the reduction of the nickel complex, (dtbbpy)$NiCl_2$ (dtbbpy = 4,4′-di-*tert*-butyl-2,2′-dipyridyl), in the presence of quinuclidine as the base, as well as the oxidation of the quinuclidine itself. Owing to the (quasi)irreversibility of the oxidation wave observed in CVs (Figure 1B), a standard thermodynamic potential cannot easily be assigned for either species. However, the onsets of the nickel reduction wave at –0.6 V as well as the quinuclidine oxidation wave at 1.1 V are in line with our proposal that the potentials of the valence and conduction bands must be balanced to allow both cathodic and anodic processes to occur. Consequently, among all the heterogeneous photocatalysts tested, metal-free $^{NH_2}CN_x$ exhibits the best performance for C–O cross-coupling.

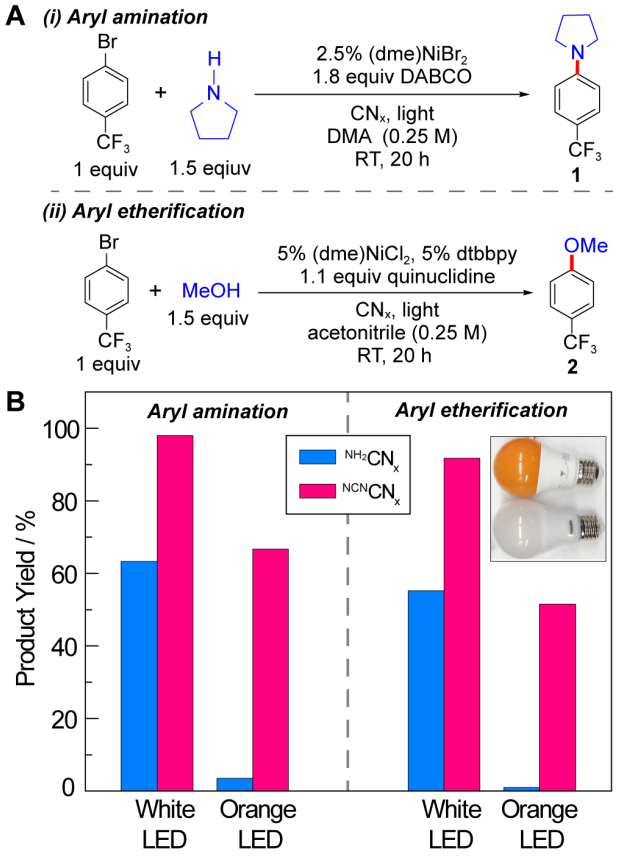

Figure 2. (**A**) Reaction conditions for nickel-catalysed aryl amination and etherification. (**B**) The product yield using photocatalyst $^{NH_2}CN_x$ or $^{NCN}CN_x$ under illumination with either white or orange LED lamps.

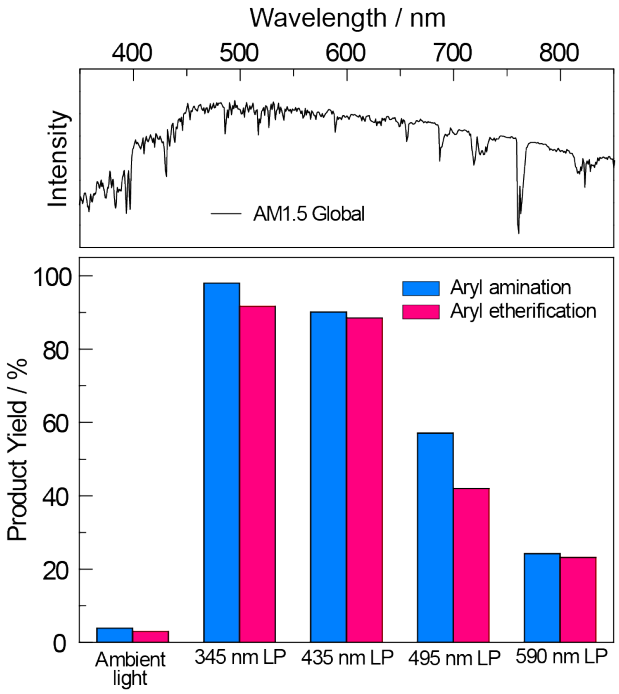

Figure 3. The product yield of nickel-catalysed aryl amination and etherification driven by broadband sunlight with $^{NCN}CN_x$ as the photocatalyst. The reactions remain active even after applying a series of long pass filters with increasing cutting wavelength up to 590 nm. AM1.5 Global solar spectrum based on ASTM G-173-03 is shown at the top for reference.

To utilize broadband sunlight, we next sought to extend the $^{NH_2}CN_x$ absorption by its chemical modification.[35,54,55] Specifically, cyanamide-modified carbon nitride ($^{NCN}CN_x$) shows not only wider absorption in the visible region than that of $^{NH_2}CN_x$ (Figure 1C)[56] but also long-lived electrons in the conduction band, which cause the material to turn blue after reductive quenching of the hole upon photolysis.[57] These long-lived electrons offer a continuous source of redox equivalents to reduce the Ni(II) complexes and drive the productive Ni(I/III) dark cycle. $^{NCN}CN_x$ was synthesized from two inexpensive precursors (melamine and potassium thiocyanate) according to a previously reported procedure (see section C in the SI).[56] The absorption edge of $^{NCN}CN_x$ is red-shifted compared to that of $^{NH_2}CN_x$, and the Tauc plot[58] shows a minor change of 60 mV in the band gap (see Figure S2). This change is likely due to a slight movement of the conduction band potential while maintain the same valence band potential.[53] Successful surface NCN functionalization was confirmed by Fourier Transform Infrared Spectroscopy (FTIR) and X-ray Photoelectron Spectroscopy (XPS) (Figures S3 and S4), which showed a cyanamide stretch and the presence of potassium, respectively, consistent with previous reports.[56] As we expected, the modified carbon nitride ($^{NCN}CN_x$) performs better as a photocatalyst than $^{NH_2}CN_x$ under all irradiation conditions (Table S1).

In analogy to aryl etherification, we posited that nickel-catalysed photoredox aryl amination could also proceed through a Ni(I/III) dark cycle given the similarity in reaction conditions.[38,39] A larger-than-one quantum yield (QY = 2.7 ± 0.1) was also reported for the C–N cross-coupling with [Ir(dF-CF_3-ppy)$_2$(dtbbpy)][PF_6] as the photocatalyst,[48] confirming the presence of a Ni(I/III) cycle, analogous to the mechanism of aryl etherification. We note that, unlike aryl etherification catalysis, aryl amination does not require dtbbpy since the amine substrate can act as a ligand to stabilize the nickel centre.

Accurate quantum yield measurements are challenging for these heterogeneous reactions owing to scattering. Consequently, we performed external quantum yield measurements (EQY = number of product / number of incident photons) for both C–N and C–O cross-coupling (see Figure 2A) using $^{NCN}CN_x$ as the photocatalyst at low incident powers. Consistent with previous observations,[47,48] we obtained EQYs in excess of unity (2.2 ± 0.2 and 2.4 ± 0.1 for C–N and C–O cross-coupling, respectively) under illumination with monochromic light at 435 nm (Section F.6 in the SI). EQY values in excess of 1 unequivocally support the existence of dark cycle, as we have previously observed. Note that the actual quantum yields should be higher because the incident photons in the EQY measurements are not all absorbed by the heterogeneous photocatalyst due to scattering.

The C–N and C–O coupling photocatalysis of the two carbon nitrides was examined using white LED and orange LED excitation (see the inset in Figure 2B and section E in the SI) under the reaction conditions shown in Figure 2A, which are similar to the optimized conditions reported previously with homogeneous photocatalysts.[38,39] For both cross-coupling reactions, $^{NCN}CN_x$ outperforms $^{NH_2}CN_x$, especially as the

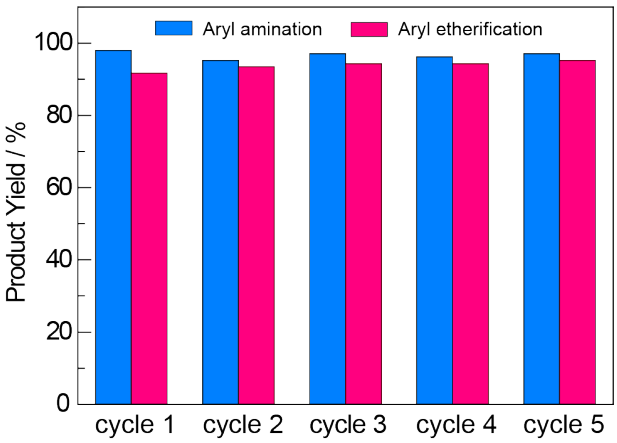

Figure 4. The $^{NCN}CN_x$. photocatalyst was reused for multiple cycles over which no decrease in product yields was observed for either aryl amination or aryl etherification.

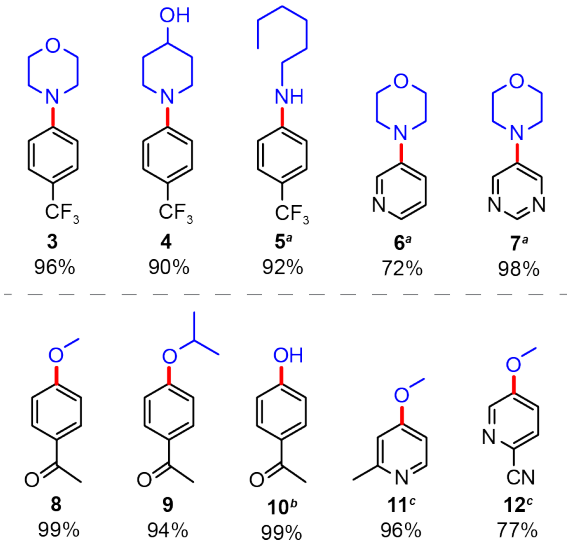

Figure 5. Applicability of nickel-catalysed aryl amination and etherification driven by sunlight and $^{NCN}CN_x$. Yields were determined by ^{1}H NMR signal referenced to 1,3-benzodioxole. [a] Reaction heated to 55 °C. [b] Different reaction condition, see section B in the SI. [c] 40 hours illumination.

excitation source is shifted into the red side of the visible absorption region. The white light LED has a spectrum peak at 460 nm in addition to a broadband emission centred at 600 nm, whereas the orange light only has the 600 nm band with no emission below 500 nm (see Figure S1). Notably, neither of the LEDs exhibit emission in the UV region. This is particularly important, because depending on the light intensity and the absorption spectrum of the photocatalyst, even a small portion of UV or blue light may be responsible for the majority of the observed activity in the presence of more intense but unproductive red light. For example, in a recent report on photoredox cross-coupling with carbon nitride,[43] the white and green light sources both contained contributions from the UV region, which appears to be responsible for the observed reactivity based on the results reported here. After 20 hours of illumination under our UV-free white light, $^{NH_2}CN_x$ resulted in product yields of 63% and 55% for the C—N and C—O couplings, respectively, in contrast to the 98% and 92% product yields observed for $^{NCN}CN_x$ (Figure 2B). Moreover, after 20-hour illumination with the orange LED light source, $^{NH_2}CN_x$ only provided a trace amount of product (3% and 1%), whereas $^{NCN}CN_x$ delivered 67% and 52% conversion for C—N and C—O couplings, respectively. These results clearly demonstrate the enhanced photoactivity of $^{NCN}CN_x$ under orange light due to its broad band absorption.

Having demonstrated the improved photoactivity of the surface-modified carbon nitride $^{NCN}CN_x$ in the visible region, the cross-coupling reactions were examined under one sun irradiance provided by a solar simulator (Newport Sol2A ABA class) with an AM1.5 filter (see section E in the SI); a 345 nm long pass filter was employed to eliminate any deep UV light. As shown in Figure 3, $^{NCN}CN_x$ drove quantitative conversions for both cross-coupling reactions. By gradually red-shifting the cut-off wavelength of the long pass filter, we observed a decrease in the product yields commensurate with the diminished absorption of $^{NCN}CN_x$. Nonetheless, even with a 590 nm long pass filter, product yields of 20% were achieved for both cross-couplings after 20 hours. These results are of particular significance since sunlight spans a broad spectrum where only a small fraction falls within the blue and UV region (see Figure 3, top panel). Thus $^{NCN}CN_x$ is able to harness an extended spectral range of sunlight (up to 590 nm) for photoredox cross-coupling reactions.

An additional advantage offered by heterogeneous photocatalysts is their facile recyclability, which is confirmed for $^{NCN}CN_x$ in Figure 4. The photocatalyst was recovered by subjecting it to three rounds of washing and centrifugation followed by drying at 130 °C in air (see section D in the SI). The recovered $^{NCN}CN_x$ showed no loss in activity after 5 cycles. Consistent with this result as wells as with previous reports[59,60] that establish the NCN surface modification to be photostable, FTIR measurements showed that the NCN surface modification was retained with photocycling (Figure S3). To further investigate whether the activity observed using recycled photocatalyst was due to residual nickel deposited on $^{NCN}CN_x$, we performed photoreactions with recycled $^{NCN}CN_x$ (after 5 cycles) in the absence of Ni^{2+} complexes. For these control experiments, we observe 4% and 0% product yield for aryl amination and etherification, respectively. Consistent with previous reports,[46] the results of these control experiments show that photocatalysis in recycling experiments is not due to nickel deposition on the $^{NCN}CN_x$ photocatalyst.

Finally, the general applicability of $^{NCN}CN_x$ was examined for the solar-driven nickel-catalysed cross-coupling between different aryl bromides and nucleophiles. For aryl amination (Figure 5), we consistently obtained the expected products with high yields for various secondary (**3, 4**) and primary (**5**) amines. Consistent with previous results, cross-coupling of heterocyclic aryl bromides proved to be more challenging,[39] but heating to 55 °C furnished product in good yields (**6, 7**). Similarly, for aryl etherification, methanol and isopropanol furnished product yields of over 90% (**8, 9**). Surprisingly, water can be cross-coupled with 99% yield under slightly modified conditions (**10**)

(see section B in SI). Heterocyclic aryl bromides were also coupled successfully in good yields with a reaction time of 40 hours (**11**, **12**).

Conclusions

We have demonstrated that surface-modified carbon nitride, $^{NCN}CN_x$, with its extended absorption in the visible region, can directly utilize broadband sunlight to drive nickel-catalysed aryl amination and etherification. In contrast to UV- and blue-light driven photoredox processes, the method disclosed herein enables highly efficient bond formation at high energy intensity (EI) while avoiding competing photoexcitations of other chemical species frequently encountered in dual photocatalytic processes. Owing to its increased efficiency in solar light absorption, metal-free nature, facile separation, ready recyclability, and straightforward synthesis, $^{NCN}CN_x$ is an attractive heterogeneous photocatalyst for environmentally benign and sustainable solar synthesis.

Acknowledgements

We want to thank Prof. Christine Caputo at University of New Hampshire for confirming the UV-vis diffuse reflectance spectrum. This work is supported by the National Science Foundation under grant CHE-1855531.

Conflicts of interest

There are no conflicts to declare.

Notes and references

1 J. M. R. Narayanam and C. R. J. Stephenson, *Chem. Soc. Rev.*, 2011, **40**, 102-113.
2 J. Xuan and W. J. Xiao, *Angew. Chem. Int. Ed.*, 2012, **51**, 6828-6838.
3 D. M. Schultz and T. P. Yoon, *Science*, 2014, **343**, 1239176.
4 M. H. Shaw, J. Twilton and D. W. C. MacMillan, *J. Org. Chem.*, 2016, **81**, 6898-6926.
5 N. A. Romero and D. A. Nicewicz, *Chem. Rev.*, 2016, **116**, 10075-10166.
6 E. C. Gentry and R. R. Knowles, *Acc. Chem. Res.*, 2016, **49**, 1546-1556.
7 C. K. Prier, D. A. Rankic and D. W. C. MacMillan, *Chem. Rev.*, 2013, **113**, 5322-5363.
8 M. D. Levin, S. Kim and F. D. Toste, *ACS Cent. Sci.*, 2016, **2**, 293-301.
9 L. Marzo, S. K. Pagire, O. Reiser and B. Konig, *Angew. Chem. Int. Ed.*, 2018, **57**, 10034-10072.
10 A. Hossain, A. Bhattacharyya and O. Reiser, *Science*, 2019, **364**, eaav9713.
11 M. N. Hopkinson, B. Sahoo, J. L. Li and F. Glorius, *Chem. Eur. J.*, 2014, **20**, 3874-3886.
12 J. K. McCusker, *Science*, 2019, **363**, 484-488.
13 K. Teegardin, J. I. Day, J. Chan and J. Weaver, *Org. Process Res. Dev.*, 2016, **20**, 1156-1163.
14 C. B. Kelly, N. R. Patel, D. N. Primer, M. Jouffroy, J. C. Tellis and G. A. Molander, *Nat. Protoc.*, 2017, **12**, 472-492.
15 A. H. Bonardi, F. Dumur, G. Noirbent, J. Lalevee and D. Gigmes, *Beilstein J. Org. Chem.*, 2018, **14**, 3025-3046.
16 B. M. Hockin, C. F. Li, N. Robertson and E. Zysman-Colman, *Catal. Sci. Technol.*, 2019, **9**, 889-915.
17 W. B. Liu, J. B. Li, P. Querard and C. J. Li, *J. Am. Chem. Soc.*, 2019, **141**, 6755-6764.
18 C. H. Lim, M. Kudisch, B. Liu and G. M. Miyake, *J. Am. Chem. Soc.*, 2018, **140**, 7667-7673.
19 J. He, C. Y. Chen, G. C. Fu and J. C. Peters, *ACS Catal.*, 2018, **8**, 11741-11748.
20 S. Ruccolo, Y. Qin, C. Schnedermann and D. G. Nocera, *J. Am. Chem. Soc.*, 2018, **140**, 14926-14937.
21 L. K. G. Ackerman, J. I. M. Alvarado and A. G. Doyle, *J. Am. Chem. Soc.*, 2018, **140**, 14059-14063.
22 B. J. Shields, B. Kudisch, G. D. Scholes and A. G. Doyle, *J. Am. Chem. Soc.*, 2018, **140**, 3035-3039.
23 S. I. Ting, S. Garakyaraghi, C. M. Taliaferro, B. J. Shields, G. D. Scholes, F. N. Castellano and A. G. Doyle, *J. Am. Chem. Soc.*, 2020, **142**, 5800-5810.
24 F. G. Calvo-Flores, *ChemSusChem*, 2009, **2**, 905-919.
25 F. Roschangar, R. A. Sheldon and C. H. Senanayake, *Green Chem.*, 2015, **17**, 752-768.
26 C. Jimenez-Gonzalez, D. J. C. Constable and C. S. Ponder, *Chem. Soc. Rev.*, 2012, **41**, 1485-1498.
27 R. P. Schwarzenbach, B. I. Escher, K. Fenner, T. B. Hofstetter, C. A. Johnson, U. von Gunten and B. Wehrli, *Science*, 2006, **313**, 1072-1077.
28 X. M. Liu, Q. J. Song, Y. Tang, W. L. Li, J. M. Xu, J. J. Wu, F. Wang and P. C. Brookes, *Sci. Total Environ.*, 2013, **463**, 530-540.
29 D. G. J. Larsson, *Philos. Trans. R. Soc. B*, 2014, **369**, 20130571.
30 D. G. Nocera, *Inorg. Chem.*, 2009, **48**, 10001-10017.
31 D. G. Nocera, *Acc. Chem. Res.*, 2017, **50**, 616-619.
32 M. Oelgemoller, *Chem. Rev.*, 2016, **116**, 9664-9682.
33 W. Y. Teoh, J. A. Scott and R. Amal, *J. Phys. Chem. Lett.*, 2012, **3**, 629-639.
34 X. J. Lang, X. D. Chen and J. C. Zhao, *Chem. Soc. Rev.*, 2014, **43**, 473-486.
35 X. C. Wang, S. Blechert and M. Antonietti, *ACS Catal.*, 2012, **2**, 1596-1606.
36 X. Li, J. G. Yu, J. X. Low, Y. P. Fang, J. Xiao and X. B. Chen, *J. Mater. Chem. A*, 2015, **3**, 2485-2534.
37 Y. Q. Qu and X. F. Duan, *Chem. Soc. Rev.*, 2013, **42**, 2568-2580.
38 J. A. Terrett, J. D. Cuthbertson, V. W. Shurtleff and D. W. C. MacMillan, *Nature*, 2015, **524**, 330-334.
39 E. B. Corcoran, M. T. Pirnot, S. S. Lin, S. D. Dreher, D. A. DiRocco, I. W. Davies, S. L. Buchwald and D. W. C. MacMillan, *Science*, 2016, **353**, 279-283.
40 E. R. Welin, C. Le, D. M. Arias-Rotondo, J. K. McCusker and D. W. C. MacMillan, *Science*, 2017, **355**, 380-384.
41 M. S. Oderinde, M. Frenette, D. W. Robbins, B. Aquila and J. W. Johannes, *J. Am. Chem. Soc.*, 2016, **138**, 1760-1763.
42 Q. M. Kainz, C. D. Matier, A. Bartoszewicz, S. L. Zultanski, J. C. Peters and G. C. Fu, *Science*, 2016, **351**, 681-684.
43 C. Cavedon, A. Madani, P. H. Seeberger and B. Pieber, *Org. Lett.*, 2019, **21**, 5331-5334.
44 I. Ghosh, J. Khamrai, A. Savateev, N. Shlapakov, M. Antonietti and B. Konig, *Science*, 2019, **365**, 360-366.
45 Y. Y. Liu, D. Liang, L. Q. Lu and W. J. Xiao, *Chem. Commun.*, 2019, **55**, 4853-4856.
46 B. Pieber, J. A. Malik, C. Cavedon, S. Gisbertz, A. Savateev, D. Cruz, T. Heil, G. G. Zhang and P. H. Seeberger, *Angew. Chem. Int. Ed.*, 2019, **58**, 9575-9580.
47 R. Sun, Y. Z. Qin, S. Ruccolo, C. Schnedermann, C. Costentin and D. G. Nocera, *J. Am. Chem. Soc.*, 2019, **141**, 89-93.

48 R. Sun, Y. Qin and D. G. Nocera, *Angew. Chem. Int. Ed.*, 2020, **59**, 2-9.
49 P. A. Payard, L. A. Perego, I. Ciofini and L. Grimaud, *ACS Catal.*, 2018, **8**, 4812-4823.
50 Y. J. Cui, Z. X. Ding, P. Liu, M. Antonietti, X. Z. Fu and X. C. Wang, *Phys. Chem. Chem. Phys.*, 2012, **14**, 1455-1462.
51 Q. P. Lu, Y. F. Yu, Q. L. Ma, B. Chen and H. Zhang, *Adv. Mater.*, 2016, **28**, 1917-1933.
52 J. Zhao, X. Wang, Z. C. Xu and J. S. C. Loo, *J. Mater. Chem. A*, 2014, **2**, 15228-15233.
53 H. Yu, R. Shi, Y. Zhao, T. Bian, Y. Zhao, C. Zhou, G. I. N. Waterhouse, L. Z. Wu, C. H. Tung and T. Zhang, *Adv. Mater.*, 2017, **29**.
54 Y. Wang, X. C. Wang and M. Antonietti, *Angew. Chem. Int. Ed.*, 2012, **51**, 68-89.
55 S. W. Cao, J. X. Low, J. G. Yu and M. Jaroniec, *Adv. Mater.*, 2015, **27**, 2150-2176.
56 V. W. Lau, I. Moudrakovski, T. Botari, S. Weinberger, M. B. Mesch, V. Duppel, J. Senker, V. Blum and B. V. Lotsch, *Nat. Commun.*, 2016, **7**, 12165.
57 H. Kasap, C. A. Caputo, B. C. M. Martindale, R. Godin, V. W. H. Lau, B. V. Lotsch, J. R. Durrant and E. Reisner, *J. Am. Chem. Soc.*, 2016, **138**, 9183-9192.
58 J. Tauc, R. Grigorovici and A. Vancu, *Phys. Stat. Sol.*, 1966, **15**, 627-637.
59 A. Vijeta and E. Reisner, *Chem. Commun. (Camb.)*, 2019, **55**, 14007-14010.
60 V. W. Lau, D. Klose, H. Kasap, F. Podjaski, M. C. Pignie, E. Reisner, G. Jeschke and B. V. Lotsch, *Angew. Chem. Int. Ed. Engl.*, 2017, **56**, 510-514.

Supporting Information

Solar-driven tandem photoredox nickel-catalysed cross-coupling using a modified carbon nitride

Yangzhong Qin,[†] Benjamin C. M. Martindale,[†] Rui Sun, Adam J. Rieth and Daniel G. Nocera*

Department of Chemistry and Chemical Biology, Harvard University, 12 Oxford Street, Cambridge, MA 02138, USA

*Email: dnocera@fas.harvard.edu

†These authors contribute equally

Table of Contents

A. General Considerations

All reagents were purchased from commercial suppliers and used without further purification. All non-deuterated solvents were purified by an argon purged solvent purification system and stored over activated 3 Å molecular sieves in a N_2-filled glovebox. Semiconductors (SiC, ZnSe, GaP and CdTe) were purchased from Sigma Aldrich and those that were not powders were ground with an agate mortar and pestle prior to use. All reaction solution preparations were performed in a N_2-filled glovebox unless otherwise stated.

B. Photoredox Reaction Solutions

For aryl amination, 0.5 mmol aryl bromide (1 equiv), 0.75 mmol amine (1.5 equiv), 12.5 μmol (dme)$NiBr_2$ (0.025 equiv), 0.9 mmol DABCO (1.8 equiv) and 0.05 mmol 1,3-benzodioxole (0.1 equiv) were placed into a 20-mL glass vial and dissolved in 2 mL of DMA as the solvent. For aryl etherification, 0.5 mmol aryl bromide (1 equiv), 0.75 mmol alcohol (1.5 equiv), 25 μmol (dme)$NiCl_2$ (0.05 equiv), 0.55 mmol quinuclidine (1.1 equiv), 25 μmol dtbbpy (0.05 equiv) and 0.05 mmol 1,3-benzodioxole (0.1 equiv) were placed into a 20-mL glass vial and dissolved in 2 mL of acetonitrile as the solvent. The solution was stirred for 30 min on a magnetic stirrer and filtered through a 0.2-μm PTFE syringe filter to furnish a clear solution which was then stored in a 20-mL vial. 8 mg (4 mg/mL) carbon nitride powder was subsequently added to the solution. All these procedures were performed in a N_2-filled glovebox. Finally, the vial was taken out of the glovebox and immediately sealed with vinyl electric tape before irradiation.

For the cross-coupling reaction between water and 4'-bromoacetophenone, 0.4 mmol 4'-bromoacetophenone (1 equiv), 0.80 mmol *N-tert*-butylisopropylamine (2 equiv), 0.02 mmol (diglyme)$NiBr_2$ (0.05 equiv), 0.02 mmol dtbbpy (0.05 equiv) and 0.05 mmol 1,3-benzodioxole (0.125 equiv) were placed in a 20-mL glass vial and dissolved in 2 mL of DMF as the solvent. The solution was stirred for 30 min and then filtered through a 0.2-μm PTFE syringe filter to yield a clear solution. Lastly, 4 mmol water (10 equiv) and 8 mg carbon nitride were added to make the final reaction mixture.

C. Carbon Nitride Preparation

Both $^{NH_2}CN_x$ and $^{NCN}CN_x$ were prepared based on a published procedure.[1] $^{NH_2}CN_x$ was prepared by heating melamine to 550 °C for 4 h under Ar and the resulting polymer was ground into a powder using an agate pestle and mortar. To prepare $^{NCN}CN_x$, the $^{NH_2}CN_x$ powder was mixed with dried KSCN in a 1:2 weight ratio. The mixture was then heated to 400 °C for 1 h and 500 °C for 0.5 h under Ar. After cooling, the polymer was ground into a powder again with a pestle and mortar. The residual KSCN was washed away by subjecting the powder to a large amount of DI water and vacuum filtration using a paper filter (Whatman 1001-070). Finally, the compound was dried at 60 °C under vacuum and ground again to furnish $^{NCN}CN_x$ powder.

D. Carbon Nitride Recycling

When each round of the reactions was completed, the reaction solutions in their original 20-mL reaction vials were centrifuged at 4400 rpm for 45 min (Eppendorf centrifuge 5702 R). A 0.1 mL aliquot of solution was then taken from the top for product yield measurement. The rest of the solution was mixed with ~20 mL acetone and shaken vigorously to re-suspend the carbon nitride. The mixture was centrifuged again at 4400 rpm for 45 min and the top clear solution was disposed. This completes the first cycle of the "washing" process. Two subsequent "washings" with ~20 mL acetone and ~20 mL ethanol were performed. After that the resulting "wet" carbon nitride was dried in an oven at 140 °C overnight. The dry recycled carbon nitride was brought into the glovebox and recharged with fresh reaction solution for the next reaction cycle.

E. Photocatalytic Reactions

To screen the heterogeneous photocatalysts (Table 1), we tested the aryl etherification reaction by placing reaction samples (maximum 2) 5 cm from a single 40 W blue light source (Kessil A160WE Tuna Blue). To compare the activity of $^{NH_2}CN_x$ and $^{NCN}CN_x$, we tested the same reaction (as shown in Table S1) with the two reaction samples situated between two identical light sources, which were two 9.5 W soft white LED A19 bulbs (Philips) or two 9 W orange LED A19 bulbs (Triglow). The distance between the edge of the sample vial and the surface of the two light bulbs was about 2 cm. For the solar-driven photoreactions, excitation was provided by a Newport Sol2A ABA class solar simulator equipped with an AM1.5 filter. The reaction samples (typically 2) were

Table S1. Photoredox aryl etherification under various conditions.

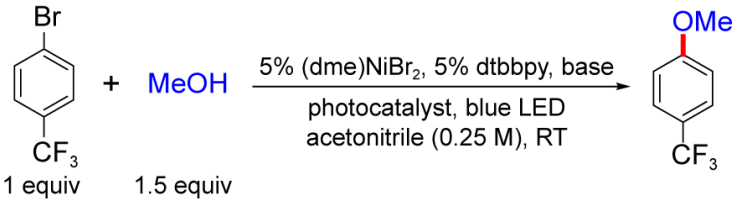

Photocatalyst	Photocatalyst Loading (mg/mL)	Reaction Time (h)	Base (equiv)	Yield (%)
$^{NH_2}CN_x$	4	24	1.1, Quin	92
$^{NCN}CN_x$	4	24	1.1, Quin	99
$^{NH_2}CN_x$	2	24	1.1, Quin	76
$^{NCN}CN_x$	2	24	1.1, Quin	98
$^{NH_2}CN_x$	2	2	1.1, Quin	23
$^{NCN}CN_x$	2	2	1.1, Quin	72
$^{NCN}CN_x$	4	24	3.0, TEA	46
$^{NCN}CN_x$	4	24	1.5, TEA	37
$^{NCN}CN_x$	4	24	1.5, DBU	17

Quin = Quinuclidine; TEA = triethylamine; DBU = 1,8-diazabicyclo[5.4.0]undec-7-ene. Yield was determined based on ^{1}H NMR signal referenced to 1,3-benzodioxole.

placed at a distance at which the light intensity was equal to one sun irradiance, as measured by a Newport 91150V solar reference cell and meter. A 5×5 in^2 filter holder fabricated by 3D printing was placed before the reaction samples so that only filtered sunlight could reach the sample. All photoreactions were run under constant stirring by a magnetic stirrer. For room temperature reactions, a high-speed fan was used to cool the sample. For reactions run at elevated temperature, the reactions samples were placed on a hotplate equipped with a thermocouple.

F. Measurements

F.1 UV-Vis Absorption and Emission Spectroscopy

The emission spectra of different lights sources (Figure S1) were measured by a CCD Array UV-vis spectrometer (SI Photonics, USA) running in the intensity mode. The measurement was carried out in a dark room. The diffuse reflectance spectra were measured with a Varian Cary 5000 UV-vis-NIR spectrometer equipped with a Praying Mantis diffuse reflection accessory (Harrick Scientific Products). The absorption spectra were constructed based on Abs = $(R_{ref} - R_{sample})/R_{ref}$, where R_{ref} and R_{sample} stands for the reflectance spectra of the reference and sample, which are PTFE powder and sample/PTFE mixed powder, respectively.

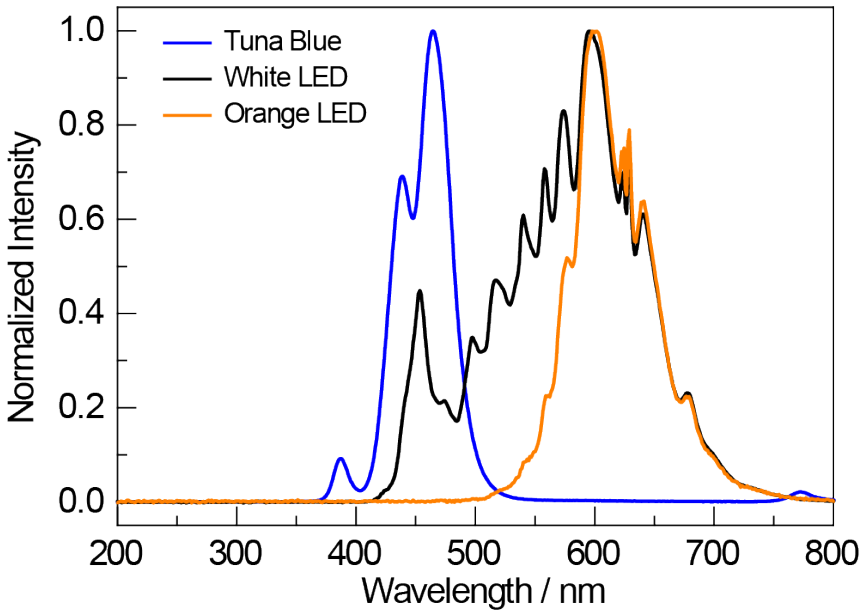

Figure S1. The emission spectra of different light sources including the Kessil A160WE tuna blue lamp (40 W), Philips soft white LED A19 bulb (9.5 W) and Triglow orange LED A19 bulb (9 W).

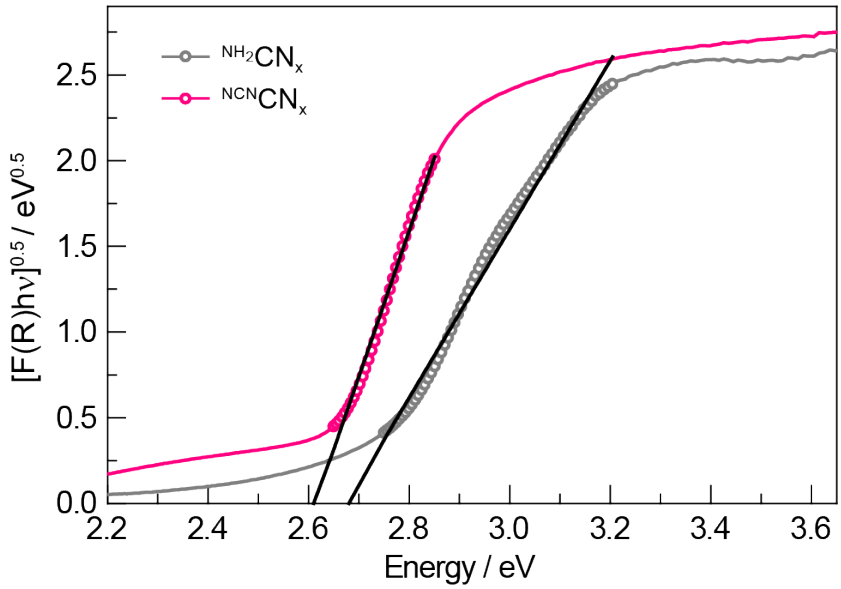

Figure S2. Tauc plot based on the diffuse reflectance, R, and the Kubelka-Munk function F(R). Selected data marked by the scattered points were fit linearly (black and red lines) to yield a band gap of 2.68 eV and 2.62 eV for $^{NH_2}CN_x$ and $^{NCN}CN_x$, respectively.

F.2 FTIR Spectroscopy

FT-IR spectra were taken on dry powder samples using a PerkinElmer Spectrum 400 FT-IR Spectrometer.

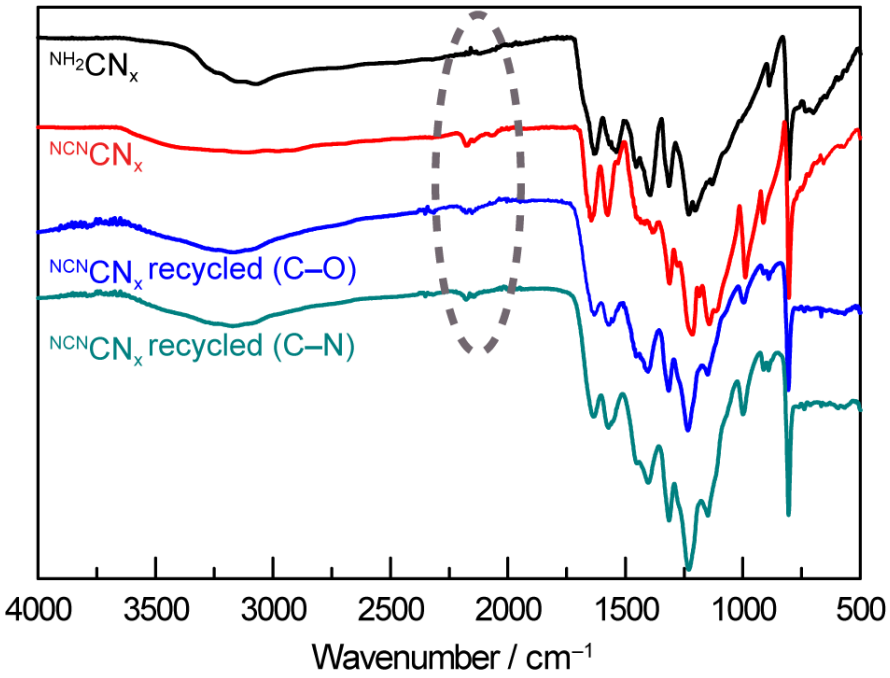

Figure S3. FTIR spectra for carbon nitride. Spectra for freshly prepared $^{NH_2}CN_x$ and $^{NCN}CN_x$ are shown in the black and red traces, respectively. Spectra for recycled $^{NCN}CN_x$ after 5 cycles of C–O and C–N coupling reactions are shown in blue and dark cyan traces, respectively. The surface modification for $^{NCN}CN_x$ is shown by the C≡N stretching band at 2177 cm^{-1} (dashed oval region), which remains after 5 cycles of reaction, indicating the photostability of the NCN surface modification.

F.3 X-Ray Photoelectron Spectroscopy

X-ray photoelectron spectroscopy (XPS) was performed at the Harvard Center for Nanoscale Systems (Cambridge, MA, USA) on a Thermo Scientific K-Alpha+ system equipped with an Al source and 180° double focusing hemispherical analyzer and 128-channel detector using a 30 µm X-ray spot size. Dry powder samples were mounted on two-sided tape on aluminum foil substrates.

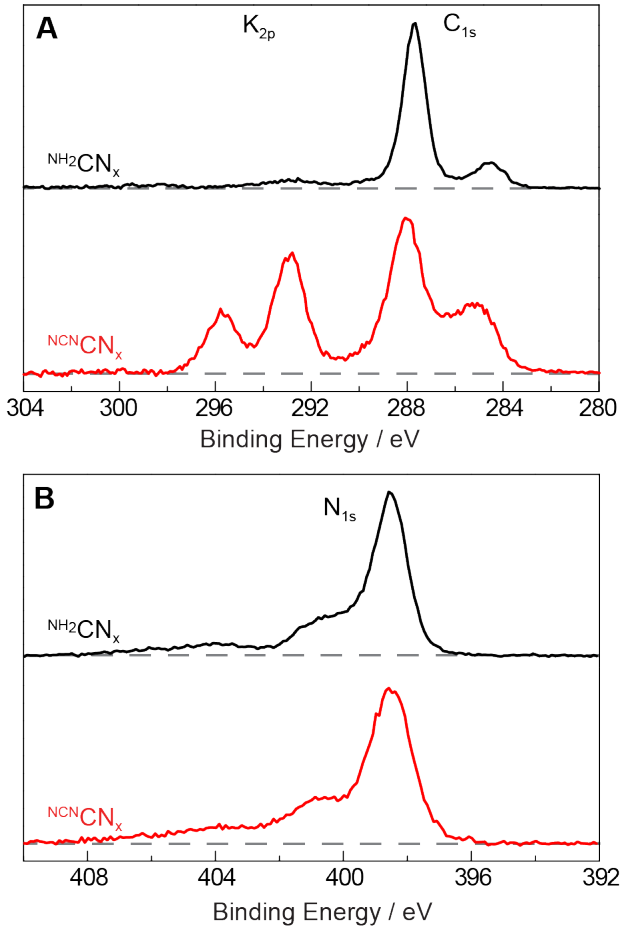

Figure S4. XPS spectra for $^{NH_2}CN_x$ and $^{NCN}CN_x$ in the region of (**A**) C_{1s} and K_{2p} (**B**) and N_{1s}. The K_{2p} signal (290-298 eV) suggests successful surface modification $^{NCN}CN_x$. The N_{1s} signal was also consistent with previous observation.[1]

F.4 NMR Spectroscopy

NMR spectra were recorded at the NMR facility located at the Harvard University Department of Chemistry and Chemical Biology. ^{1}H or ^{19}F spectra were collected on an Agilent DD2 spectrometer (600 MHz) or a Varian/Inova spectrometer (500 MHz). The reaction solutions were made with proteo-solvents (DMA, acetonitrile or DMF) containing pre-quantified 1,3-benzodioxole as the internal standard. To prepare the NMR samples, a 0.1 mL aliquot of reaction solution was mixed with 0.8 mL $CDCl_3$, and the solution was filtered and then placed in an NMR tube.

F.5 Cyclic Voltammetry

Cyclic voltammetry (CV) measurements were carried out with a CH Instruments (CHI) potentiostat 760D and Version 10.03 software in a nitrogen filled glovebox. The compounds were dissolved in either acetonitrile or DMA with 0.1 M *n*-Bu_4NBF_4 as the electrolyte. A three-electrode configuration was used with a glassy carbon working electrode, Pt wire counter electrode and non-aqueous Ag/Ag^+ reference electrode. All glassy carbon working electrodes were polished on felt using 3-µm and 1-µm diamond pastes before use. The CV of a 1 mM ferrocene (Fc) solution was taken at the beginning of each experiment as a reference.

F.6 External Quantum Yield Measurement

The external quantum yield (EQY) was measured for both C–N and C–O cross-couplings (see Figure 2A in the main text) using the following formula,

$$EQY = \frac{number\ of\ product\ molecule}{number\ of\ incident\ photon} = \frac{cV}{\emptyset t}$$

where c is concentration of product, V is the volume of the reaction solution, $\emptyset$ is the photon flux and t is the reaction time. For each measurement, 1.5 mL of solution (see Section B) and 6 mg $^{NCN}CN_x$ were placed in a 1 cm path length cuvette and illuminated by monochromic light provided by a 150 W Xe arc lamp (Newport 67005 arc lamp housing and 69907 power supply) and a 435 nm band pass filter (FWHM = 10 nm). The light was focused onto the sample by a focusing lens (f = 40 mm). The power was adjusted by a neutral density filter and measured by an Ophir ORION/PD power meter and PD-300-ROHS head sensor. The photon flux was further calibrated to be 4.21×10^9 mol/s (corresponding to a power of 1.16 mW) by ferrioxalate based on a published procedure.[2] The product concentration was determined by ^{1}H NMR spectrum referenced to 1,3-benzodioxole as an internal standard. The reactions were run three times to furnish an average quantum yield and standard deviation.

G. References

(1) Lau, V. W.; Moudrakovski, I.; Botari, T.; Weinberger, S.; Mesch, M. B.; Duppel, V.; Senker, J.; Blum, V.; Lotsch, B. V. Rational Design of Carbon Nitride Photocatalysts by Identification of Cyanamide Defects as Catalytically Relevant Sites. *Nat. Commun.* **2016**, *7*, 12165.

(2) Hatchard, C. G.; Parker, C. A. A New Sensitive Chemical Actinometer-II. Potassium Ferrioxalate as a Standard Chemical Actinometer. *Proc. R. Soc. London, Ser. A* **1956**, *235*, 518-536.